Research Article | Vol. 32, No. 6 / 11 Mar 2024 / Optics Express 9644

Optics EXPRESS

High-Q Tamm plasmon-like resonance in spherical Bragg microcavity resonators

YALINA GARCÍA-PUENTE,[1,*] BAPTISTE AUGUIÉ,[2] AND RAMAN KASHYAP[1,3]

[1]Department of Physics Engineering, École Polytechnique Montréal, 2900 Édouard-Montpetit, Montréal, Qc H3 T 1J4, Canada
[2]The MacDiarmid Institute for Advanced Materials and Nanotechnology School of Chemical and Physical Sciences, Victoria University of Wellington, Wellington 6140, New Zealand
[3]Department of Electrical Engineering, PolyGrames, École Polytechnique Montréal, 2900 Édouard-Montpetit, Montréal, Qc H3 T 1J4, Canada
[*]yalina-2.garcia-puente@polymtl.ca

Abstract: This work proposes what we believe to be a novel Tamm plasmon-like resonance supporting structure consisting of an Au/SiO_2 core-shell metal nanosphere structure surrounded by a TiO_2/SiO_2 spherical Bragg resonator (SBR). The cavity formed between the core metal particle and the SBR supports a localized mode similar to Tamm plasmons in planar dielectric multilayers. Theoretical simulations reveal a sharp absorption peak in the SBR bandgap region, associated with this mode, together with strong local field enhancement. We studied the modification of a dipolar electric emitter's radiative and non-radiative decay rates in this resonant structure, resulting in a quantum efficiency of ~90% for a dipole at a distance of $r = 60$ *nm* from the Au nanosphere surface. A 30-layer metal-SBR Tamm plasmon-like resonant supporting structure results in a Q up to $\sim 10^3$. The Tamm plasmon-like mode is affected by the Bragg wavelength and the number of layers of the SBR, and the thickness of the spacer cavity layer. These results will open a new avenue for generating high-Q Tamm plasmon-like modes for switches, optical logic computing devices, and nonlinear applications.

1. Introduction

Over the past few decades, there has been extensive research into the interaction of resonant light and metal nanostructures, resulting in remarkable advancements in manipulating optical intensity at scales well below the wavelength of light [1,2]. Surface plasmon resonances (SPRs) facilitate this interaction by harnessing the coherent oscillations of conduction electrons, resulting in an accumulation of induced charges at the metal surface, along with significant enhancements in the local field [1,3]. Various design approaches, such as micro-disks, spherical resonators, metallic gratings, Au nanopillars, and nanoparticle arrays, have been proposed to achieve high-Q resonances and minimize radiative and Ohmic losses [4–8]. Plasmon resonances have been shown to enhance light-matter interactions in various applications of interest, ranging from photochemistry to high-harmonic generation, plasmonic nano-ovens and photodetection, as well as improve sensing and light management applications [9–14].

Tamm plasmon polaritons (TPPs) are a type of hybrid plasmonic–dielectric resonance that have recently gained significant attention due to their exclusive properties and potential for practical applications [15]. Tamm plasmon polaritons are generally defined as an electromagnetic mode confined between a dielectric mirror or Bragg reflector and a terminating metallic boundary. This asymmetric structure may be seen as a cavity surrounded by two mirrors, or equivalently, with the resulting mode having a mixed photonics–dielectric character; the enhanced electromagnetic field decays very rapidly inside the metal layer, while the field penetration into the DBR affords the resonance a much higher quality factor than with surface plasmon resonance platforms

#514259 https://doi.org/10.1364/OE.514259
Journal © 2024 Received 23 Nov 2023; revised 22 Jan 2024; accepted 16 Feb 2024; published 4 Mar 2024

Optics EXPRESS

[16,17]. This field confinement leads to substantial field enhancement and sensitive environmental response. Unlike conventional surface plasmon resonances, TPPs can be directly excited at normal incidence, making them a promising alternative to standard SPs. Tamm plasmons have many potential applications, including absorbers, lasers, switches, sensors, solar photovoltaic cells, photo-catalysis, filters, and others [10,15,18–20].

Photonic crystals (PCs) have shown great potential for developing high-Q electromagnetic resonances, paving the way for their implementation in photonic and optoelectronic devices [4]. In Tamm plasmon research, a frequently used class of plasmonic nanostructure is a distributed Bragg reflector (DBR) coated with a thin metal layer. DBRs consist of layers with alternating high and low refractive indices with an optical thickness of about one-quarter wavelength [21–23]. However, recent experimental studies by *Yang et al*. have demonstrated that employing a thicker metal layer under the DBR can yield a higher Q-factor ~20 [24,25]. Furthermore, introducing a defect layer into the DBR structure has enabled the observation of TPPs modes with $FWHM \sim 2\ nm$ and $Q \sim 778$ at the near-infrared region [26]. The original TPP structure was one-dimensional (1D), with a planar multilayer. These structures are relatively easy to fabricate, but limit the electric field confinement to 1D (the axis of the multilayer stack). In order to maximize light-matter interaction, a three-dimensional (3D) confinement is ideally required, which may be achieved by patterning the metal layer to further confine the TPP mode [4,27].

Alternatively, we propose here a novel Tamm plasmon-supporting configuration that is intrinsically 3D and spherically symmetric. We investigate the near-infrared scattering properties of a SBR Tamm-like structure, obtained by surrounding an Au/SiO_2 core-shell metal nanosphere structure with a TiO_2/SiO_2 SBR. The SBR exhibits resonant modes with high-quality factor and small modal volume [28–30] and has been shown to successfully manipulate electrical and magnetic quantum emitters for optical amplification and lasing [31,32]. By including a metal nanoparticle at the centre of the structure, a new electromagnetic mode can be confined at the metal–SBR interface. Our theoretical model predicts a sharp absorption peak in the SBR bandgap window, which can be attributed to the coupling of light with a TPP-like mode confined between the core metal nanosphere and the surrounding SBR. Additionally, we examine a dipolar magnetic emitter's radiative and non-radiative decay rates and find a quantum efficiency of approximately ~90% for a dipole at a distance of $r = 60\ nm$ from the Au nanosphere surface. We predict that a 30-layer SBR with an Au/SiO_2 core-shell metal nanosphere structure yields TPP modes with a high-quality factor of up to $\sim 10^3$. Furthermore, we observe that the TPP induced in the structure depends mainly on the number of layers (N), the Bragg wavelength of the SBR, and the thickness of the defect cavity layer. These findings suggest that high-Q TPP-like modes can be excited in a spherical geometry, with intriguing characteristics that may find applications for nano-lasing and other resonantly-enhanced light-matter interactions at the nanoscale. At present, the fabrication of such structures seems relatively difficult [33,34], but the same type of resonance could also be observed in larger structures in a different wavelength range, allowing easier fabrication methods such as 3D-printing [29].

2. Theory of light scattering by multilayered spherical plasmonic nanoparticles

Metallic nanoparticles (NPs) have unique properties due to their size, particularly when compared to metal skin depth. At this size range, the electric field of incoming light can penetrate the metal and polarize the conduction electrons leading to collective oscillations [35,36]. One fascinating property of these NPs is the emergence of localized surface plasmons (LSPs), non-propagating excitations distributed over the entire particle volume. The frequency of the plasmon resonance can be controlled by altering the dielectric properties of the surrounding medium or the NP's size, shape, and composition [2]. This resonant interaction with light is illustrated in Fig. 1, showing the calculated absorbance of an Au/SiO_2 core-shell nanosphere placed in air with a spacer cavity thickness of $t_{cavity} = 239\ nm$ and different Au radii, $r_{core} = 20$ nm, $r_{core} = 30\ nm$

Optics EXPRESS

and r_{core} = 40 *nm*. The absorbance curves peak at around 520 *nm* – 550 *nm*, related to the Au nanosphere's localized surface plasmon resonance (LSPR). The schematic view of the Au/SiO_2 core-shell nanosphere is also depicted.

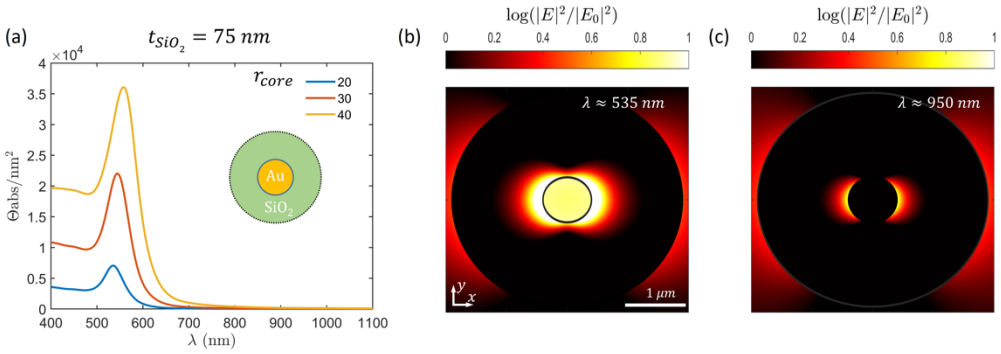

Fig. 1. (a) Calculated Au/SiO_2 core-shell nanosphere absorbance with spacer cavity shell thickness t_{cavity} = 239 *nm* and different Au radius r_{core}. (Inserted) Schematic view of the Au/SiO_2 core-shell nanosphere. Normalized electric field intensity $|E|^2/|E_0|^2$ in (b) with $\lambda \approx 535$ *nm* and (c) $\lambda \approx 950$ *nm*.

To further illustrate the plasmonic resonances and the electric field enhancement at the surface of the Au/SiO_2 core-shell nanosphere, the electric field distribution of the Au/SiO_2 nanosphere at $\lambda \approx 530$ *nm* and $\lambda \approx 950$ *nm* were simulated and depicted in Fig. 1(b) and (c), respectively. The electric field strength is normalized to its maximum value. At the LSPR wavelength ~530 nm, the increased absorption substantially enhanced the electric field around the Au nanosphere. Interband transitions are the primary mechanism that causes loss in these gold nanoparticles in the high-energy end of the visible spectrum. This process involves exciting single particles from the occupied 5d valence band to the vacant levels of the 6s-6p conduction band in gold [37]. On the other hand, at $\lambda \approx 950$ *nm*, the electric field distribution is more uniform and weaker. At these long wavelengths, Au can be characterized by the Drude model since it follows the behavior of free electron metals [2].

This study will emphasize a Tamm-like structure composed of a core-shell Au/SiO_2 nanoparticle and a Spherical Bragg Resonator (SBR) in the near-infrared (NIR) region where the intrinsic damping of Au is reduced. The complex dielectric function reported in [38] for Au and refractive index of n_L = 1.44 for SiO_2 [39] and n_H = 1.75 for TiO_2 [25] were utilized to conduct the theoretical calculations.

Our theoretical model follows the treatment of SBRs described in [31], using the transfer matrix method. Transfer matrices are commonly used to describe analytically the scattering properties of multilayered spherical structures, and efficient codes are available for their computation [40]. We make use of the relationship between *T*-matrix and *S*-matrix [40] to determine the *S*-matrix coefficients:

$$\bar{\bar{S}} \equiv \bar{\bar{I}} + 2\bar{\bar{T}} \tag{1}$$

where $\bar{\bar{I}}$ is the identity matrix.

The *S*-matrix is diagonalized due to the spherical geometry of our structures, which can be represented by the decoupling of electric and magnetic multipoles of order l in spherical coordinates. Thus, the *S*-matrix fully characterizes the scattering process for each multipole l and diagonal component p. Working with the *S*-matrix is advantageous as it enables direct identification of electromagnetic modes that can be excited in the structure. Specifically, we apply a Weierstrass factorization to each component p, corresponding to two singularities: poles

Optics EXPRESS

and zeros [41]. Poles represent eigenmodes, while zeros are associated with perfect absorption [42], and their position describes the scattering properties of the system [41].

The normalized radiative decay rate (Γ) of a dipole located at the core center in multilayer spheres can be estimated using this transfer matrix by [43,44]:

$$\frac{\Gamma_{\perp}}{\Gamma_0} = \frac{3}{2x_d^4}\frac{n_d}{n_{host}}\sum_l l(l+1)(2l+1)|f_{El}(x_d)|^2 \tag{2}$$

$$\frac{\Gamma_{\parallel}}{\Gamma_0} = \frac{3}{4x_d^4}\frac{n_d}{n_{host}}\sum_l (2l+1)[|f_{Ml}(x_d)|^2 + |f'_{El}(x_d)|^2] \tag{3}$$

where "$\perp$" and "||" correspond to the perpendicular and parallel orientation of the dipole located at position d, n_{host} is the refractive index of the host medium, l is the angular quantum number, and $f_{\mathrm{El,Ml}}(\mathrm{x_d})$ are linear combinations of Riccati-Bessel functions multiplied by expansion coefficients determined through raising and lowering composite transfer matrices, while the prime represents the differentiation with respect to the argument [43,44]. The dimensionless size parameter is defined by $\mathrm{x_d} = k_\mathrm{d} r_\mathrm{d}$ where $k_\mathrm{d} = 2\pi n_\mathrm{d}/\lambda$.

Also, for the case where a plane wave illuminates the SBR, the total absorption can be obtained from the S or T matrices as [43,44]:

$$\theta_{abs} = \frac{\pi}{2k^2}\sum_{p,l}(2l+1)|1-S_{pl}|^2 = \frac{\pi}{2k^2}\sum_{p,l}(2l+1)(1-|1+2T_{pl}|^2) \tag{4}$$

where k is the wave vector.

For independent validation of the results, we have also used the MATLAB package SPLAC by Etchegoin and Le Ru, which implements a slightly different recursive algorithm for multilayered spheres, also based on Mie theory [45,46]. The accuracy of these algorithms for solving the Maxwell equations in different spherical multilayer plasmonic structures has been widely demonstrated in previous works [25,47]. In our experience, the results of both codes show excellent agreement in simple structure, and in far-field cross-sections, but for near-field calculations involving many layers and high-quality resonances, the STRATIFY code appears to suffer from numerical instabilities, and we therefore relied on SPLAC for these near-field calculations.

3. Results and discussion

The 3D Tamm-like structure we propose is composed of a core-shell metal nanosphere structure embedded at the center of a SBR (metal-SBR), as sketched in Fig. 2(a). The core-shell structure consists of a gold core surrounded by a SiO_2 shell with radii of $r_{core} = 20\ nm$ and $t_{cavity} = 239\ nm$, respectively. The TiO_2/SiO_2 SBR surrounding the core-shell structure is designed to act as a Bragg mirror at the Bragg wavelength $\lambda_B \approx 950\ nm$. The SBR shell thickness was fixed at $L_{SiO2} = \lambda_B/4n_L = 163.79\,nm$ and $L_{TiO2} = \lambda_B/4n_H = 135.71\,nm$. A plane wave propagating in the x direction and linearly polarized along z is used as the excitation source and the host medium is air ($n_\mathrm{host} = 1$).

The absorption characteristics of the Tamm-like structure were analyzed by varying the number of SBR layers from $N = 10$ to $N = 30$, and the results are presented in Fig. 2(b). The calculated absorbance of the metal–SBR structure presents a sharp peak in the absorption cross-section, with maximum amplitude reaching $\sim 10^4 nm^2$, at around $\lambda \approx 900\ nm$. We attribute this distinctive spectral feature to the excitation of a Tamm plasmon-like mode, confined between the spherical Bragg reflector and the metal core nanosphere. Note that this resonance wavelength is far detuned from the localized plasmon resonance of the core-shell particle (Fig. 1, resonance at 535 nm); this new mode has a distinct character, involving both photonic and plasmonic features. As the number of SBR layers increases, the absorption increases, and the peak becomes narrower.

Optics EXPRESS

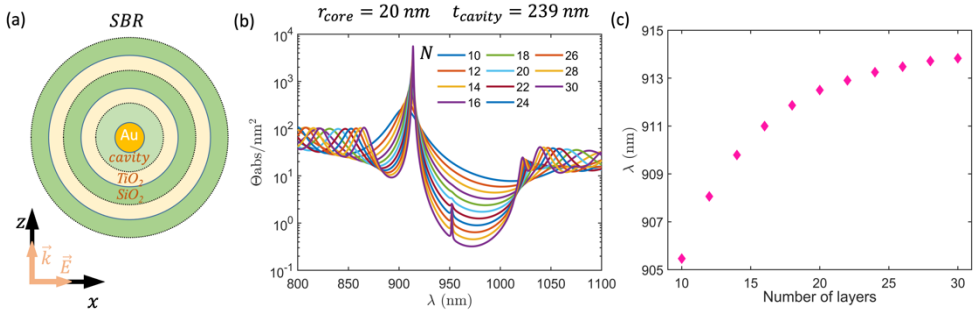

Fig. 2. (a) Schematic view of the proposed Tamm plasmon-like resonance supporting structure, composed of a TiO_2/SiO_2 SBR with an Au/SiO_2 core-shell metal nanosphere structure in the core. (b) Calculated absorbance of the Tamm plasmon-like resonance supporting structure of Au radius $r_{core} = 20\ nm$, spacer cavity shell thickness $t_{cavity} = 239\ nm$, and Bragg wavelength $\lambda_B \approx 950\ nm$ excited by a plane wave varying the number of the SBR layers from 10 to 30. (c) Wavelength dependence of the maximum absorption with the number of SBR layers.

Importantly, the absorption maximum in this metal-SBR structure coincides with a large increase in the electromagnetic field. Furthermore, another peak starts to be noticeable around $\lambda \approx 950\ nm$ when the number of SBR layers exceeds $N = 20$. The increased absorption with the number of SBR layers also indicates the potential for achieving higher-Q plasmonic microcavities. These findings are promising for various applications, such as sensing and optoelectronics.

The wavelength dependence of the maximum absorption with the number of SBR layers is presented in Fig. 2(c). It is observed that the absorption maximum of the metal-SBR moves towards higher frequencies as the number of SBR layers increases. This shift is attributed to the introduction of a phase change between the reflected wave by the SBR and by the metal core, thereby influencing the observed absorption behavior.

In the following, we will concentrate on a Tamm-like structure consisting of an Au/SiO_2 core-shell nanosphere of radius $r_{core} = 20\ nm$ and shell thickness $t_{cavity} = 239\ nm$, surrounded by a 30-layer TiO_2/SiO_2 SBR with Bragg wavelength $\lambda_B \approx 950\ nm$. A detailed study of their eigenmodes was performed to obtain the resonant condition of the metal-SBR structure. Figure 3 presents the maps obtained of the S_{pl} matrix component of order $l = 1$ and $l = 2$ in the complex frequency plane for TE and TM polarization. The circumferences in the maps indicate the two lowest-order modes of the structure, namely TE1 and TM2. It is observed that the absorption maximum of the metal-SBR structure coincides with the electric dipole core mode TE1 of the structure. The electric dipole mode TE1 is a Tamm-like mode that is confined between the Au core and the TiO_2/SiO_2 SBR. This agrees with the result presented in Fig. 2(b) and corroborates that the absorption peak at around $\lambda \approx 913\ nm$ is due to the excitation of a Tamm-like mode. On the other hand, with the other absorption peak observed at $\lambda \approx 950\ nm$ in Fig. 2(b) is identified as the magnetic quadrupole mode TM2.

In order to illustrate the Tamm-like mode's influence on a dipole emitter, namely the loss and local density of states, Fig. 4 presents the radiative decay rate enhancement of an electric dipole in the spacer layer of the 30-layer TiO_2/SiO_2 metal-SBR structure at a distance of $r = 22\ nm$ from the Au nanosphere surface. Figure 4(a) shows the perpendicular and parallel components of the radiative and non-radiative decay rates up to $l = 5$ and $l = 20$, plotted as solid and dashed lines, respectively. The perpendicular and parallel components of the radiative and non-radiative decay rates are directly proportional to the local density of states. The results shows a peak $\lambda \approx 913\ nm$ in the perpendicular and parallel components of the decay rate and another peak at $\lambda \approx 950\ nm$ in the parallel component. The increased radiative decay rate indicates that the metal-SBR structure

Optics EXPRESS

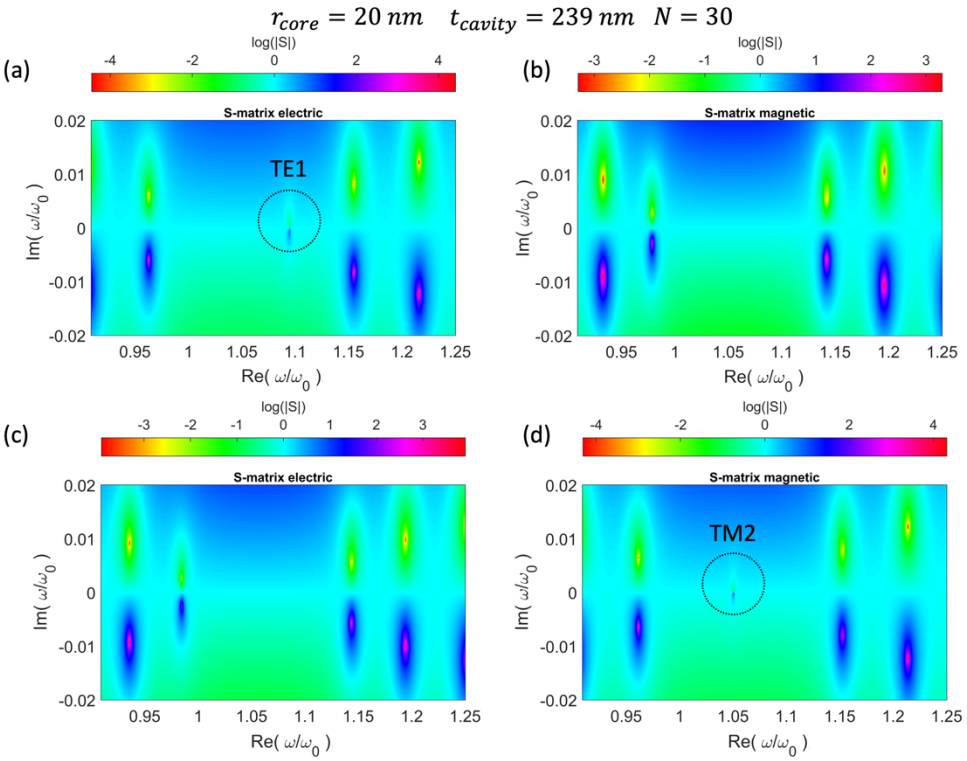

Fig. 3. Maps of the S_{pl} matrix component of order $l = 1$ and $l = 2$ in the complex frequency plane for TE (a,b) and TM (c,d) polarization. The Tamm plasmon-like resonance supporting structure comprises an Au core with radius $r_{core} = 20\ nm$ and a SiO_2 spacer cavity shell thickness $t_{cavity} = 239\ nm$, surrounded by a 30-layer TiO_2/SiO_2 SBR with Bragg wavelength $\lambda_B \approx 950\ nm$. The circumferences signal the structure's two lowest-order modes, TE1 and TM2.

promotes dipole emission, which is directly related to the enhanced electromagnetic field. It is also observed that there is no significant difference in the radiative decay rate between the $l = 5$ and $l = 20$, which implies that the performed calculation converged.

In particular, Figs. 4(b) and (c) show the dipole $l = 1$ and quadrupole $l = 2$ contributions to the perpendicular and parallel components of the radiative decay rate increase. Notably, the maximum at $\lambda \approx 913\ nm$ nm coincides with the TE1 mode obtained in Fig. 3. In addition, the maximum in the $l = 2$ dipolar contribution of the radiative decay rate coincides with the magnetic quadrupole mode TM2. Overall, these results provide further evidence of the enhanced electromagnetic field in the metal-SBR structure, which promotes these dipole and quadrupolar emissions.

In Fig. 5(a), we can see the dependence of the radiative and non-radiative decay rate enhancement on the distance of the dipole from the Au nanosphere surface at $\lambda \approx 913\ nm$. It is observed that the enhancement of radiative and non-radiative decay rates is of the order of $\sim 10^2$ and $\sim 10^3$, respectively, for positions of the dipole near the Au nanosphere surface $r = 22\ nm$. This suggests that the metal-SBR structure enhances the decay rate of the dipole by at least one order of magnitude, which can have important implications for various applications such as sensing and lasing. Moreover, it is interesting to note that the distinction between the parallel and perpendicular components of the decay rate enhancement diminishes as we move farther from the

Optics EXPRESS

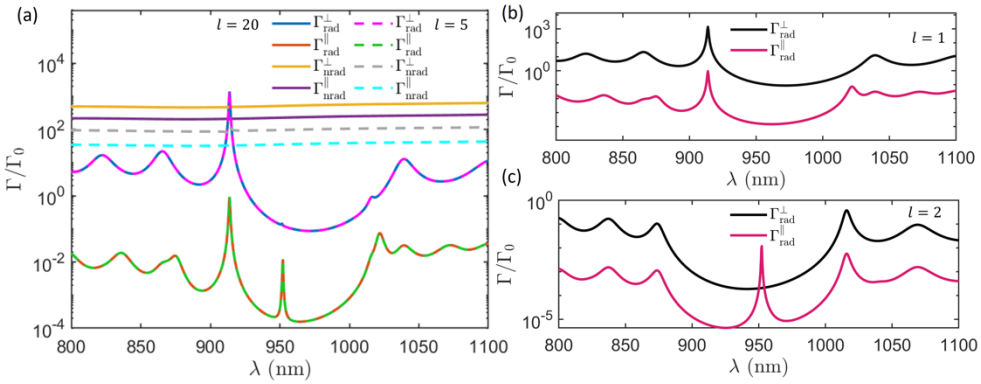

Fig. 4. Radiative decay rate enhancement of an electric dipole placed in the cavity (spacer) shell of the 30-layer TiO_2/SiO_2 SBR at $r = 22$ *nm* from the surface of the Au core nanosphere. (a) Perpendicular and parallel components of the radiative and nonradiative decay rates up to other $l = 5$ and $l = 20$ are plotted as solid and dotted lines, respectively. (b) Dipolar $l = 1$ and (c) quadrupolar $l = 2$ contribution to perpendicular and parallel components of the radiative decay rate enhancement.

surface of the Au nanosphere. The difference between the parallel and perpendicular components becomes negligible, indicating that the enhancement does not depend on the dipole's orientation.

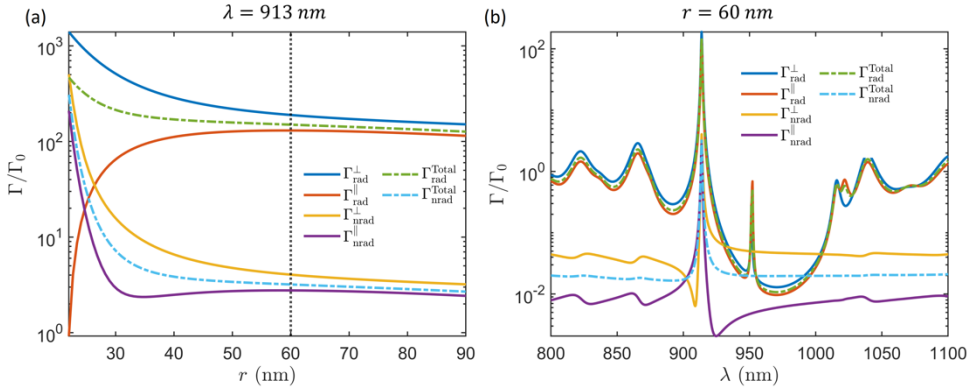

Fig. 5. (a) Perpendicular, parallel, and total radiative and nonradiative decay rate enhancement dependency on the dipole distance from the Au nanosphere surface r at $\lambda \approx 930$ *nm*. (b) Radiative decay rate enhancement of an electric dipole in the spacer shell of the metal-SBR structure at $r = 60$ *nm* from the surface of the Au nanosphere.

The previously reported decrease in the nonradiative decay rate for $r = 22$ *nm* ensures the possibility of improving the quantum efficiency ($\eta = \Gamma_{rad}/\Gamma_{rad} + \Gamma_{nrad}$) of a dipole placed in that region. In particular, for $r = 60$ *nm*, the dipolar quantum efficiency is approximately ~0.9, and Fig. 5(b) shows the radiative and nonradiative decay rate for this case. As noted, a maximum is observed at TE1 and TM2 frequencies, confirming the results obtained in Fig. 4.

The decay rate enhancement for increasing numbers of layers in the TiO_2/SiO_2 SBR, with an Au radius of $r_{core} = 20$ *nm* and a spacer cavity shell thickness of $t_{cavity} = 239$ *nm*, is depicted in Fig. 6(a). A maximum in the decay rate is appreciated at the TE1 dipole resonance wavelength. Its value increases, and the bandwidth becomes narrower as the number of layers increase. Furthermore, a second peak is also noticed at the TM2 resonance frequency. In addition, the

Optics EXPRESS

enhanced decay rate stripes observed at wavelengths above $\lambda \approx 1050\ nm$ and around $\lambda \approx 825\ nm$ correspond to higher-order magnetic resonance modes. They are of the whispering gallery mode (WGM) type, as confirmed by near-field maps (not shown).

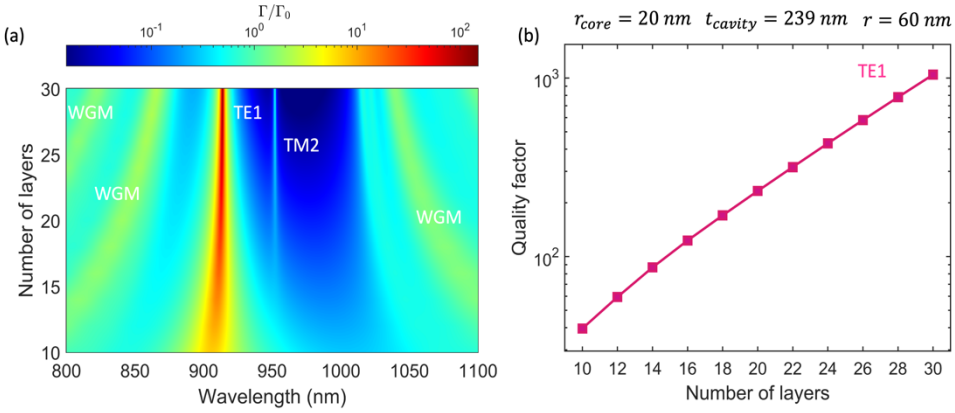

Fig. 6. (a) Decay rate enhancement as a function of the number of layers of the TiO_2/SiO_2 SBR with Au radius core $r_{core} = 20\ nm$, spacer cavity shell thickness $t_{cavity} = 239\ nm$, and Bragg wavelength $\lambda_B \approx 950\ nm$. The dipolar electric and magnetic resonances are labeled by TE1 and TM1, respectively. (b) Calculated quality factor for a spherical Bragg resonator with a different number of layers at TE1 ≈913 *nm*.

The calculated quality factor $Q = \omega_0/\Delta\omega$ for the electric resonant dipole mode TE1 ($\lambda \approx 913\ nm$) in the spherical Bragg resonator as a function of different layers is shown in Fig. 6(b). A nonlinear relation between the quality factor and the number of layers was found. The results suggest that it is possible to obtain plasmonic Tamm modes with quality factors of $Q \approx 10^3$ or even higher by coupling an Au nanosphere with an SBR. Such values are comparable to the quality factor of electric resonant dipole modes in SBR and the well-known whispering gallery modes, but here the mode volume is confined to the region immediately outside the core metal nanosphere. These findings are crucial as they demonstrate the possibility of strong coupling between an electric dipole and the plasmonic resonances in an metal-SBR structure. The results also highlight the significance of the number of layers in the metal-SBR structure in achieving high-quality plasmonic Tamm modes. We note that, similarly to the planar case, there will be a critical coupling condition [30] leading to maximum absorption, though for the parameters of this study the absorption simply increases with the number of layers.

As demonstrated in planar structures, choosing the materials and geometrical parameters is a key factor for TPP resonance [17,21,25]. Figure 7 shows the calculated absorbance of the Au structure as a function of the spacer cavity shell thickness and Bragg wavelength. In Fig. 7(a), the radius of the Au core is fixed at $r_{core} = 20\ nm$, and the number of layers is $N = 30$, with a Bragg wavelength of approximately $\lambda_B \approx 950\ nm$. As the thickness of the SiO_2 spacer cavity layer increases, the absorbance at the TE1 resonance frequency also increases, and the maximum peak of the absorbance shifts towards longer wavelengths. This shift can be attributed to the change in optical path length in the effective cavity defined between the metallic core and the enclosing SBR.

On the other hand, in Fig. 7(b), the spacer cavity shell thickness is fixed at $t_{cavity} = 239\ nm$, and the absorbance is plotted as a function of the wavelength for different values of the Bragg wavelength λ_B, which corresponds to different SBR layer thicknesses. When the Bragg wavelength is changed, an adjustment in the thicknesses of the SBR layers is intrinsically required, leading to a shift in the effective refractive index of the cavity mode. This modification of the refractive

Optics EXPRESS

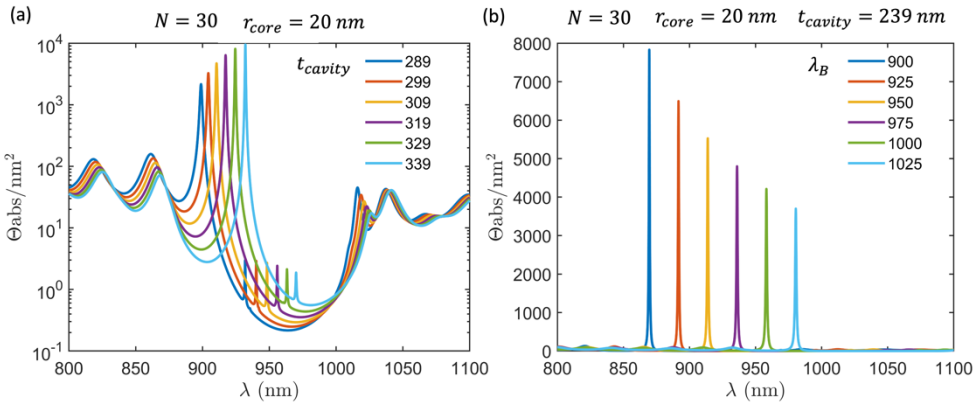

Fig. 7. (a) The calculated absorbance of the metal-SBR structure with an Au radius $r_{core} = 20\ nm$, $N = 30$, and Bragg wavelength $\lambda_B \approx 950\ nm$, varying the spacer cavity shell thickness from $t_{cavity} = 289\ nm$ to $t_{cavity} = 339\ nm$ and (b) for different Bragg wavelengths λ_B and spacer cavity shell thickness $t_{cavity} = 239\ nm$.

index directly influences the resonant condition of the cavity, resulting in the observed wavelength shift of the resonant mode.

Overall, the results highlight the critical role of fine-tuning the thickness of the spacer cavity layer and the Bragg wavelength for optimizing the absorbance of Tamm-like structures. By carefully adjusting these parameters, achieving high absorbance at specific resonant frequencies is possible, which can be helpful for various applications in photovoltaics, sensing, and other light-matter applications relying on high local fields, 3D confinement, and small mode volume. We believe that our findings are expected to pave the way for developing novel plasmonic devices with improved performance and high-quality factor plasmonic resonances.

This paper proposes a novel Tamm plasmon-like resonance supporting structure by coupling an Au/SiO_2 core-shell metal nanosphere structure with a TiO_2/SiO_2 SBR. In Fig. 8, the calculated electric field intensity distribution at $\lambda = 911\ nm$ is presented for the metal-SBR structure, where the Au/SiO_2 core-shell nanosphere of radius $r_{core} = 20\ nm$ and shell thickness $t_{cavity} = 239\ nm$, surrounded by a 30-layer TiO_2/SiO_2 SBR with Bragg wavelength $\lambda_B \approx 950\ nm$. Note the use of a logarithmic scale on the y-axis, as the local field is amplified by 3 orders of magnitude immediately outside the metal core (the incident plane wave is taken with a unit field amplitude $|E_0| = 1$). These near-field calculations were performed using the SPLAC MATLAB package [45,46], which is an implementation of Mie theory for multilayered spheres focusing on nanophotonics and near-field applications. We found excellent agreement between both codes in far-field calculations, however the STRATIFY code appears to suffer from numerical instabilities in near-field calculations. The inserted image provides a closer view around the Au nanoparticle, with vertical dotted lines denoting the interfaces between layers. The examined mode is highly localized near the Au particle, with a field profile exhibiting evanescent decay on both sides of the metal/dielectric interface, akin to Tamm plasmon polaritons observed in conventional multilayered planar structures [16,17] and the multilayered cylindrical system proposed by C. E. Little et al. [48]. The field profile within the Bragg layers decays rapidly but presents more complex intensity fluctuations than in a planar configuration.

The achievement of a Tamm-like mode with a low-index dielectric adjacent to the metal is very intriguing, particularly when contrasted with the behavior observed in planar geometries. In the planar multilayer geometry, the cavity layer between DBR and metal must be of high refractive index, to allow the existence of a Tamm plasmon mode. In the case of a low refractive index

Optics EXPRESS

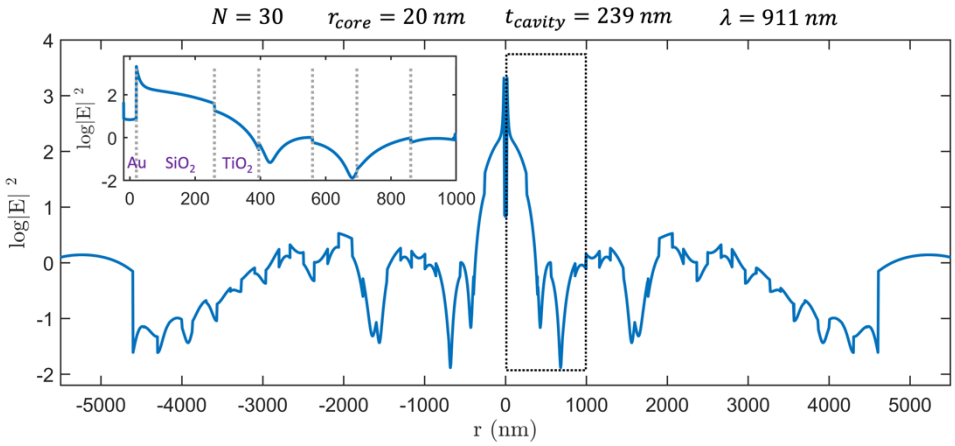

Fig. 8. Calculated electric field intensity distribution of the metal-SBR structure with an Au radius $r_{core} = 20\ nm$, $N = 30$, Bragg wavelength $\lambda_B \approx 950\ nm$, and spacer cavity shell thickness $t_{cavity} = 239\ nm$ at $\lambda = 911\ nm$. Inserted figure: Zoom around the Au nanoparticle, the vertical dotted lines denote the layers interface.

cavity, the presence of sharper absorbance has been attributed to a coupling between the cavity mode and a TPP mode [49]. Here, both high-index or low-index cavities allow the existence of a confined mode resembling a Tamm plasmon, in the spherical geometry. We have focused on the low-index cavity case, but the high-index configuration shows similar features, albeit at a different resonance wavelength. One potential explanation is that, unlike planar geometries, the spherical symmetry of the SBR allows for separating electric and magnetic components and introduces the possibility of distinct phase-matching conditions for each polarization. While the term "Tamm-like mode" has been employed in this work to describe the modes, due to the obvious analogy with the planar geometry, it becomes apparent that their exact character will require a deeper analytical exploration to fully understand how the phase matching condition characterizing planar TPPs translates in the spherical geometry. This revelation adds a layer of complexity to the behavior of SBRs, necessitating further investigation to comprehend their intricacies fully.

This questions surrounding the nature and connection of the observed modes in our SBRs to the original Tamm plasmon concept underscores the richness and complexity of these 3D cavity structures. Our work sheds light on the unique characteristics of SBRs and catalyzes future research endeavors to unravel their potential applications in photonics, optoelectronics, and various related fields. As we continue to explore the intricacies of SBRs, we advance our understanding of these resonant modes and pave the way for innovative technological applications, thus driving progress in advanced electromagnetic emission engineering and lasing applications.

4. Conclusions

Our theoretical investigation has proposed a novel Tamm-like resonance supporting structure with promising optical properties. The coupling of an Au/SiO_2 core-shell metal nanosphere structure with a TiO_2/SiO_2 SBR results in a TPP-like mode that induces a peak in the SBR bandgap region due to the coupling between the localized plasmon resonance of the core metal particle and defect modes in the SBR. Our results demonstrate that the TPP-like mode characteristics depend on the Bragg wavelength, the number of layers of the SBR, and the thickness of the defect cavity layer. The study also finds that a dipole's radiative and non-radiative decay rates at a distance of $r = 60\ nm$ from the Au nanosphere surface result in a high quantum efficiency of ~90%. A

Optics EXPRESS

30-layer metal-SBR structure also yields TPP-like modes with a high-quality factor of up to $\sim 10^3$, making this structure a potential candidate for switches, optical logic computing devices, and nonlinear applications. Overall, our work opens a new avenue for generating high-Q TPP-like modes and provides valuable insights into the design and optimization of resonant nano-spherical structures for various applications in photonics and optoelectronics.

Funding. Natural Sciences and Engineering Research Council of Canada (Discovery grants, Strategic Research grants).

Acknowledgment. R. Kashyap acknowledges financial support for the Canadian NSERC Discovery grants and Strategic Research grants programs.

Disclosures. The authors declare no conflicts of interest.

Data availability. Data underlying the results presented in this paper are not publicly available at this time but may be obtained from the authors upon reasonable request.

References

1. S. A. Maier, *Plasmonics: fundamentals and applications* (Springer, 2007), Vol. 1.
2. V. Amendola, R. Pilot, M. Frasconi, *et al.*, "Surface plasmon resonance in gold nanoparticles: a review," J. Phys.: Condens. Matter **29**, 203002 (2017).
3. J. A. Polo Jr and A. Lakhtakia, "Surface electromagnetic waves: a review," Laser Photonics Rev. **5**(2), 234–246 (2011).
4. B. Wang, P. Yu, W. Wang, *et al.*, "High-Q plasmonic resonances: fundamentals and applications," Adv. Opt. Mater. **9**(7), 2001520 (2021).
5. B. Min, E. Ostby, V. Sorger, *et al.*, "High-Q surface-plasmon-polariton whispering-gallery microcavity," Nature **457**(7228), 455–458 (2009).
6. M. G. Silveirinha, "Trapping light in open plasmonic nanostructures," Phys. Rev. A **89**(2), 023813 (2014).
7. X. Yang, G. Xiao, Y. Lu, *et al.*, "Narrow plasmonic surface lattice resonances with preference to asymmetric dielectric environment," Opt. Express **27**(18), 25384–25394 (2019).
8. W. Zhou and T. W. Odom, "Tunable subradiant lattice plasmons by out-of-plane dipolar interactions," Nat. Nanotechnol. **6**(7), 423–427 (2011).
9. J.-Y. Jing, Q. Wang, W.-M. Zhao, *et al.*, "Long-range surface plasmon resonance and its sensing applications: A review," Opt. Lasers Eng. **112**, 103–118 (2019).
10. A. Philip and A. R. Kumar, "The performance enhancement of surface plasmon resonance optical sensors using nanomaterials: A review," Coord. Chem. Rev. **458**, 214424 (2022).
11. S. A. Pillai and M. Green, "Plasmonics for photovoltaic applications," Sol. Energy Mater. Sol. Cells **94**(9), 1481–1486 (2010).
12. L. Wang, M. Hasanzadeh Kafshgari, and M. Meunier, "Optical properties and applications of plasmonic-metal nanoparticles," Adv. Funct. Mater. **30**(51), 2005400 (2020).
13. M. A. García, "Surface plasmons in metallic nanoparticles: fundamentals and applications," J. Phys. D: Appl. Phys. **44**(28), 283001 (2011).
14. L. Meng, R. Yu, M. Qiu, *et al.*, "Plasmonic nano-oven by concatenation of multishell photothermal enhancement," ACS Nano **11**(8), 7915–7924 (2017).
15. C. Kar, S. Jena, D. V. Udupa, *et al.*, "Tamm plasmon polariton in planar structures: A brief overview and applications," Opt. Laser Technol. **159**, 108928 (2023).
16. M. Sasin, R. Seisyan, M. Kalitteevski, *et al.*, "Tamm plasmon polaritons: Slow and spatially compact light," Appl. Phys. Lett. **92**(25), 251112 (2008).
17. M. Kaliteevski, I. Iorsh, S. Brand, *et al.*, "Tamm plasmon-polaritons: Possible electromagnetic states at the interface of a metal and a dielectric Bragg mirror," Phys. Rev. B **76**(16), 165415 (2007).
18. N. Bellassai, R. D'Agata, V. Jungbluth, *et al.*, "Surface plasmon resonance for biomarker detection: advances in non-invasive cancer diagnosis," Front. Chem. **7**, 570 (2019).
19. I. A. Shelykh, A. V. Kavokin, Y. G. Rubo, *et al.*, "Polariton polarization-sensitive phenomena in planar semiconductor microcavities," Semicond. Sci. Technol. **25**(1), 013001 (2010).
20. S. Tsintzos, N. Pelekanos, G. Konstantinidis, *et al.*, "A GaAs polariton light-emitting diode operating near room temperature," Nature **453**(7193), 372–375 (2008).
21. B. Auguié, M. C. Fuertes, P. C. Angelomé, *et al.*, "Tamm plasmon resonance in mesoporous multilayers: toward a sensing application," ACS Photonics **1**(9), 775–780 (2014).
22. A. M. Ahmed and A. Mehaney, "Ultra-high sensitive 1D porous silicon photonic crystal sensor based on the coupling of Tamm/Fano resonances in the mid-infrared region," Sci. Rep. **9**(1), 6973 (2019).
23. E. Buzavaite-Verteliene, I. Plikusiene, T. Tolenis, *et al.*, "Hybrid Tamm-surface plasmon polariton mode for highly sensitive detection of protein interactions," Opt. Express **28**(20), 29033–29043 (2020).
24. Z.-Y. Yang, S. Ishii, T. Yokoyama, *et al.*, "Narrowband wavelength selective thermal emitters by confined Tamm plasmon polaritons," ACS Photonics **4**(9), 2212–2219 (2017).

Optics EXPRESS

25. B. Auguié, A. Bruchhausen, and A. Fainstein, "Critical coupling to Tamm plasmons," J. Opt. **17**(3), 035003 (2015).
26. H. Lu, Y. Li, H. Jiao, *et al.*, "Induced reflection in Tamm plasmon systems," Opt. Express **27**(4), 5383–5392 (2019).
27. C. Symonds, G. Lheureux, J. P. Hugonin, *et al.*, "Confined Tamm plasmon lasers," Nano Lett. **13**(7), 3179–3184 (2013).
28. G. Burlak, S. Koshevaya, J. Sanchez-Mondragon, *et al.*, "Electromagnetic eigenoscillations and fields in a dielectric microsphere with multilayer spherical stack," Opt. Commun. **187**(1-3), 91–105 (2001).
29. Y. García-Puente, J.-J. Laurin, and R. Kashyap, "Photomic crystals," in *Frontiers in Optics*, (Optica Publishing Group, 2019), FTu6B. 4.
30. Y. Xu, W. Liang, A. Yariv, *et al.*, "Modal analysis of Bragg onion resonators," Opt. Lett. **29**(5), 424–426 (2004).
31. Y. García-Puente and R. Kashyap, "Spherical Bragg resonators for lasing applications: a theoretical approach," Opt. Express **30**(26), 47720–47732 (2022).
32. Y. García-Puente and R. Kashyap, "Magnetic Purcell Enhancement in a Nanoantenna-Spherical Bragg Resonator Coupled System," Ann. Phys. **1**, 2300147 (2023).
33. H. Shibata, K. Imakita, and M. Fujii, "Fabrication of a core–shell–shell particle with a quarter-wave thick shell and its optical properties," RSC Adv. **4**(61), 32293–32297 (2014).
34. A. V. Medvedev, A. A. Dukin, N. A. Feoktistov, *et al.*, "Spherical distributed Bragg reflector with an omnidirectional stop band in the near-IR spectral range," Semiconductors **53**(7), 901–905 (2019).
35. P. K. Jain, X. Huang, I. H. El-Sayed, *et al.*, "Review of some interesting surface plasmon resonance-enhanced properties of noble metal nanoparticles and their applications to biosystems," Plasmonics **2**(3), 107–118 (2007).
36. T. Klar, M. Perner, S. Grosse, *et al.*, "Surface-plasmon resonances in single metallic nanoparticles," Phys. Rev. Lett. **80**(19), 4249–4252 (1998).
37. M. G. Blaber, M. D. Arnold, and M. J. Ford, "A review of the optical properties of alloys and intermetallics for plasmonics," J. Phys.: Condens. Matter **22**(44), 143201 (2010).
38. E. D. Palik, *Handbook of optical constants of solids* (Academic press, 1998), Vol. 3.
39. B. Brixner, "Refractive-index interpolation for fused silica," J. Opt. Soc. Am. **57**(5), 674–676 (1967).
40. C. F. A. H. Bohren and D. R. , *Absorption and scattering of light by small particles* (Wiley-Interscience, New York, 1998).
41. V. Grigoriev, A. Tahri, S. Varault, *et al.*, "Optimization of resonant effects in nanostructures via Weierstrass factorization," Phys. Rev. A **88**(1), 011803 (2013).
42. A. Krasnok, D. Baranov, H. Li, *et al.*, "Anomalies in light scattering," Adv. Opt. Photonics **11**(4), 892–951 (2019).
43. A. Moroz, "A recursive transfer-matrix solution for a dipole radiating inside and outside a stratified sphere," Ann. Phys. **315**(2), 352–418 (2005).
44. I. L. Rasskazov, P. S. Carney, and A. Moroz, "STRATIFY: a comprehensive and versatile MATLAB code for a multilayered sphere," OSA Continuum **3**(8), 2290–2306 (2020).
45. E. Le Ru and P. Etchegoin, "SPlaC package v1. 0 guide and supplementary information," Victoria University, Tech. Rep (2008).
46. E. Le Ru and P. Etchegoin, "SERS and plasmonics codes (SPlaC)," MATLAB codes freely available from http://www.vuw.ac.nz/raman/book/codes.aspx (2009).
47. I. L. Rasskazov, A. Moroz, and P. S. Carney, "Extraordinary fluorescence enhancement in metal-dielectric core-shell nanoparticles," J. Phys. Chem. Lett. **12**(27), 6425–6430 (2021).
48. C. Little, R. Anufriev, I. Iorsh, *et al.*, "Tamm plasmon polaritons in multilayered cylindrical structures," Phys. Rev. B **86**(23), 235425 (2012).
49. Z. Wang, J. K. Clark, Y.-L. Ho, *et al.*, "Narrowband thermal emission realized through the coupling of cavity and Tamm plasmon resonances," ACS Photonics **5**(6), 2446–2452 (2018).